Supplementary Materials

Synergistic design and synthesis of O, N Co-doped hierarchical porous carbon for enhanced supercapacitor performance

Hongwei Liu[1,2,3], Zhenming Cui[1,2,3], Yan Sun[1,2,3], Zhennan Qiao[1,2,3], Yanlan Zhang[1,2,3], Qiang Bai[1], Yongzhen Wang[1,2,3,*]

[1]College of Materials Science and Engineering, Taiyuan University of Technology, Taiyuan 030024, Shanxi, China.

[2]State Key Shanxi Joint Laboratory of Coal-based Solid Waste Resource Utilization and Green Development, Taiyuan University of Technology, Taiyuan 030024, Shanxi, China.

[3]Innovation Research Center for Materials Genetic Engineering, Taiyuan University of Technology, Taiyuan 030024, Shanxi, China.

[*]**Correspondence to:** Prof. Yongzhen Wang, College of Materials Science and Engineering, Taiyuan University of Technology, 79 Yingze West Main Street, Taiyuan 030024, Shanxi, China. E-mail: wangyongzhen@tyut.edu.cn

MATERIAL AND METHODS

Sample data collection

The required data are derived from experimental results in the literature on N, O co-doped porous carbon materials (PCMs) in supercapacitor electrodes. The data collection process is carried out using several keywords, such as "N-doped porous carbon", "porous carbon", "coal-derived porous carbon", and their combination with "specific capacitors", "supercapacitors" and "electrodes". It should be noted that there are many characteristic factors that affect the performance of supercapacitors, but many of them are only internal comparisons through the graph, or there is no specific data, no unified standard, and even no report of some characteristic factors, which brings great challenges to capacitance prediction. To this end, the information of N, O co-doped porous carbon samples includes as much as possible microstructure characteristics, N and O functional group strength and operating parameters. Multiple raw datasets were collected, from which 69 nearly defect-free datasets were filtered and input values were screened in detail. Extraction data related to N, O co-doping as a carbon electrode material were provided in Table 2 of Supplementary[1-11]. Therefore, the potential window was 0.8~1 V, the current density was 0.1 ~ 1 A g^{-1}, the electrolyte was 6 M KOH, and ten structural features of N, O co-doped PCMs including specific surface area (SSA), S_{mic}, ratio of N, O, C, ratio of N/O species were extracted as suitable features for predicting the capacitance of N, O co-doped PCMs. Figures 1 and 2 of Supplementary show the histograms and curves of the normal density of capacitance and the associated porous structure characteristics, respectively. The distribution of capacitance is normally distributed, and the distribution of the 12 variables approximates a normal or lognormal distribution.

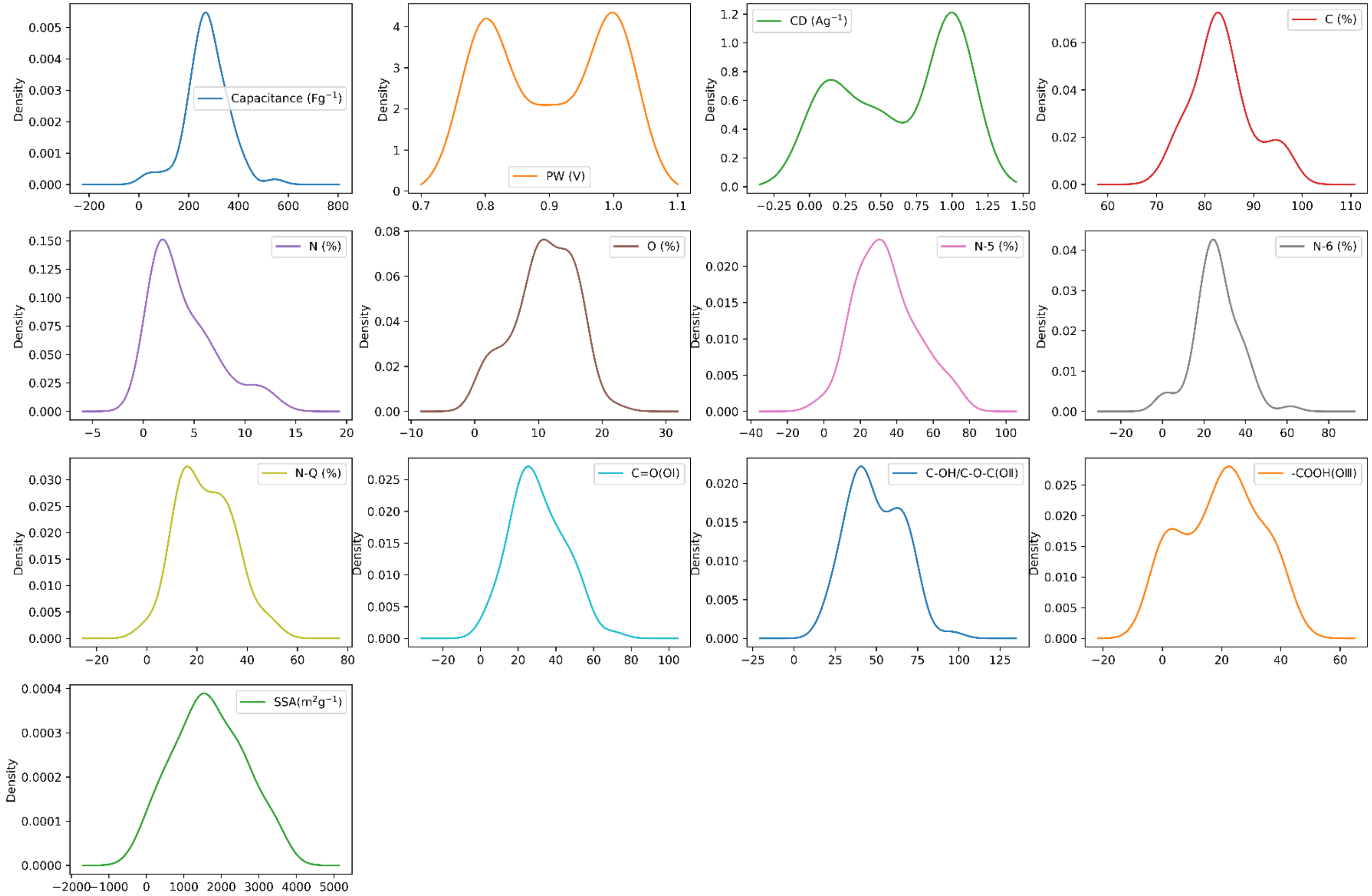

Figure 1. Histogram of frequency distribution and curve of normal density of capacitance and individual features.

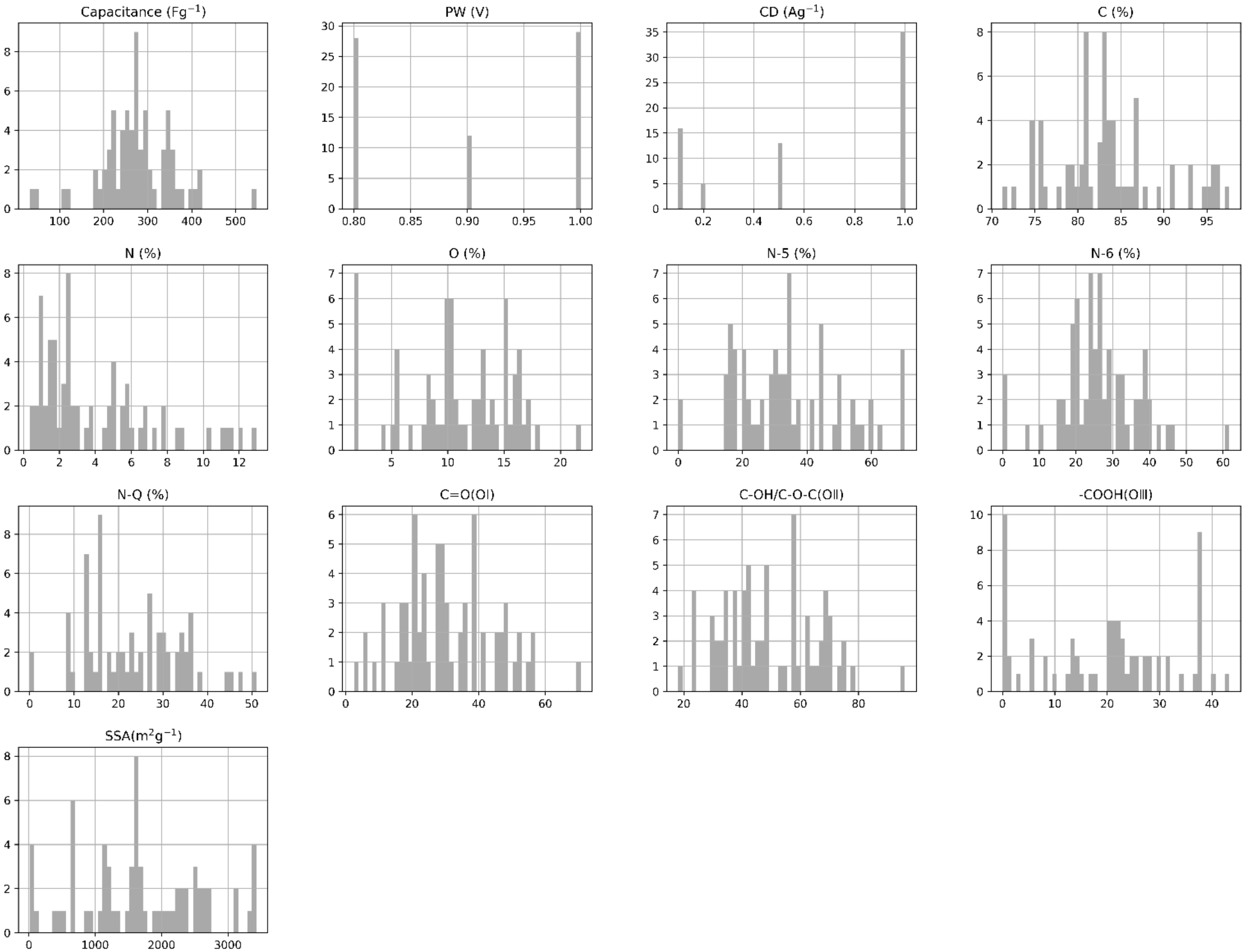

Figure 2. Histogram of frequency distribution of capacitance and individual features.

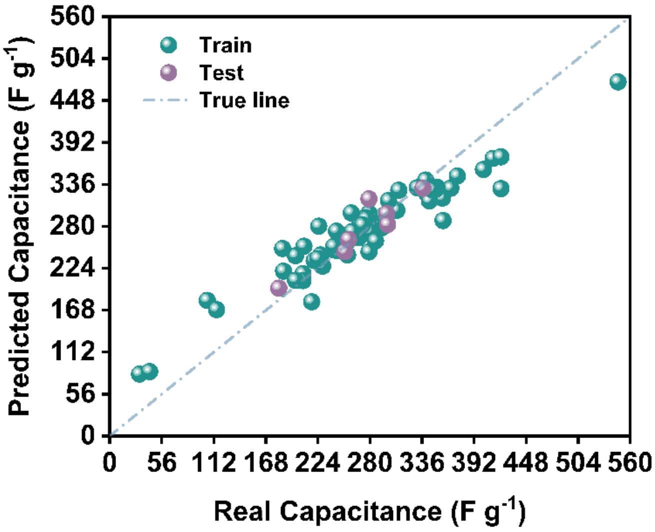

Figure 3. Prediction diagrams for all data sets of the RF model. Points closer to the baseline indicate more accurate predictions and points further away from the baseline indicate greater errors. The solid line represents the equality of predicted capacitance and real capacitance.

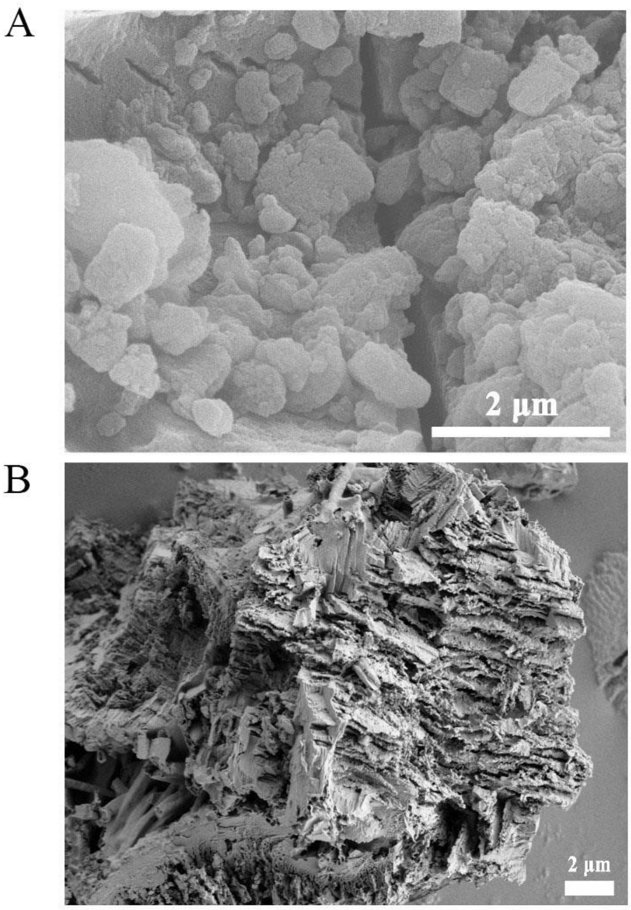

Figure 4. SEM images of (A) pre-treated lignite and (B) g-C_3N_4.

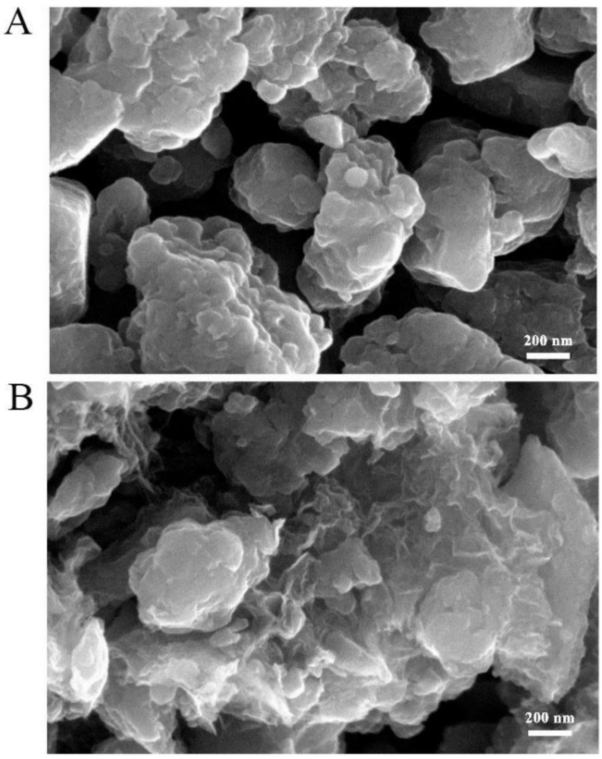

Figure 5. SEM images of (A) OPC-900 and (B) NPC-900.

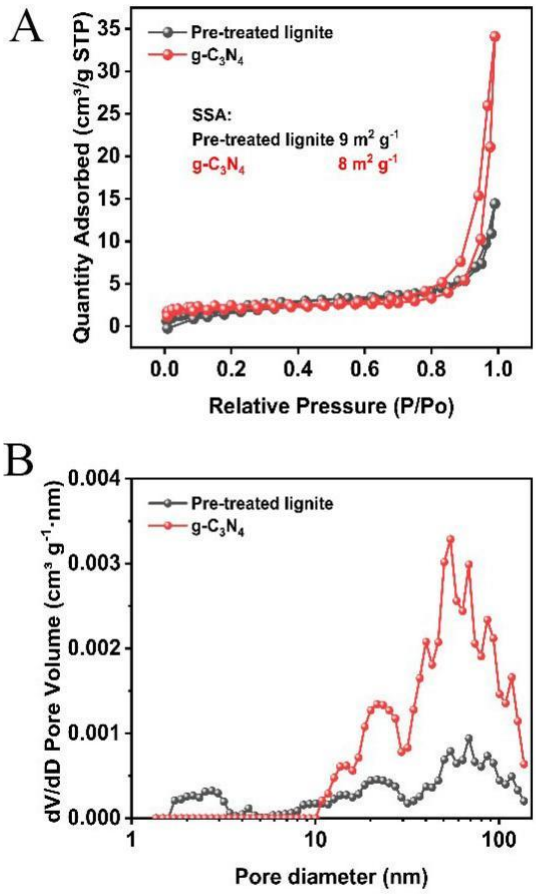

Figure 6. (A) N_2 adsorption-desorption isotherms; (B) Pore sizes distribution of pre-treated lignite and g-C_3N_4.

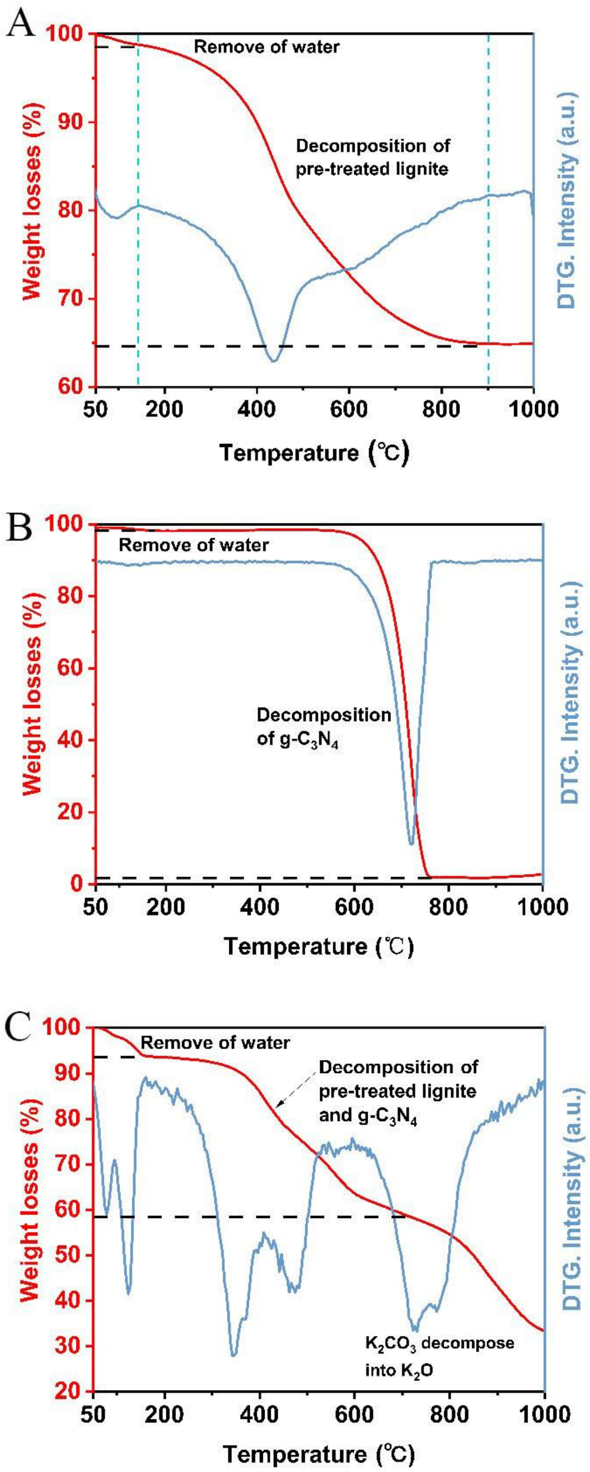

Figure 7. TGA and DTG curves of (A) pre-treated lignite, (B) g-C_3N_4, and (C) ball milling the precursor of ONPC materials, respectively.

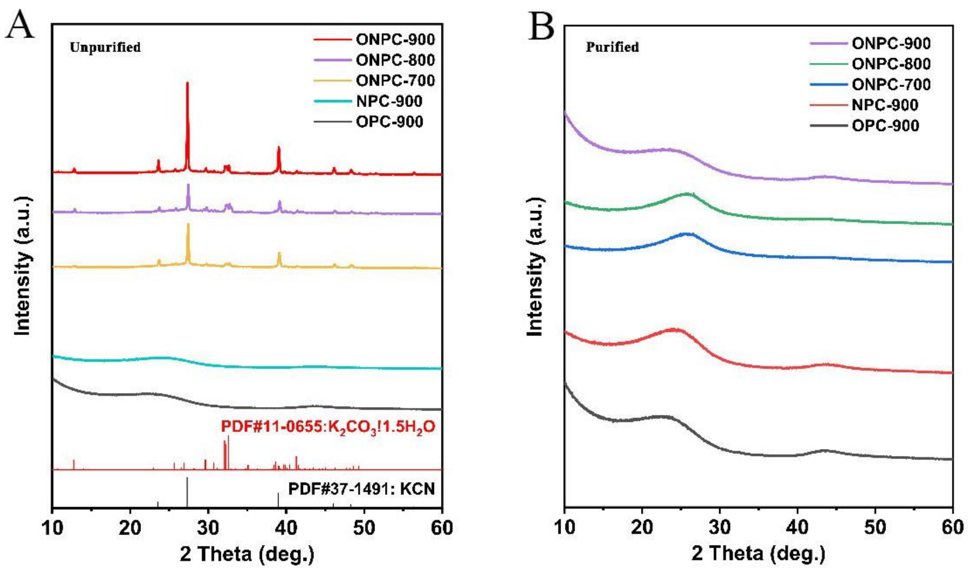

Figure 8. XRD patterns of all obtained (A) unpurified and (B) purified ONPC materials.

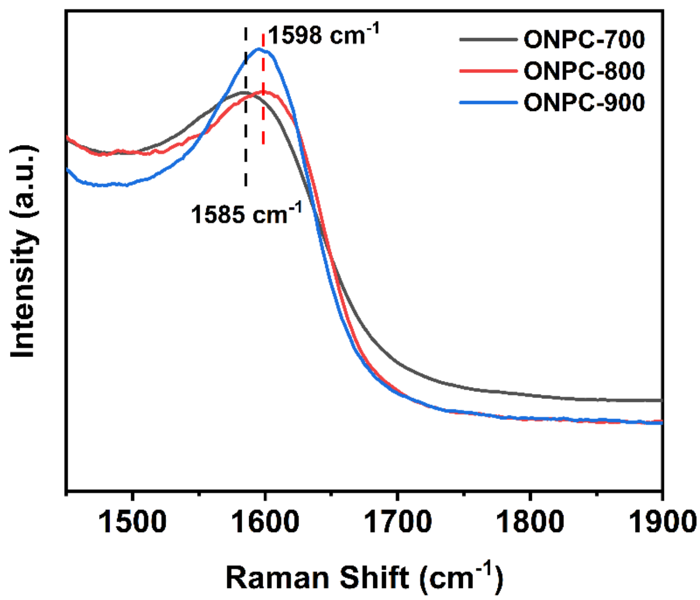

Figure 9. Local magnification of the NOPC-700, NOPC-800, and NOPC-900 Raman spectra.

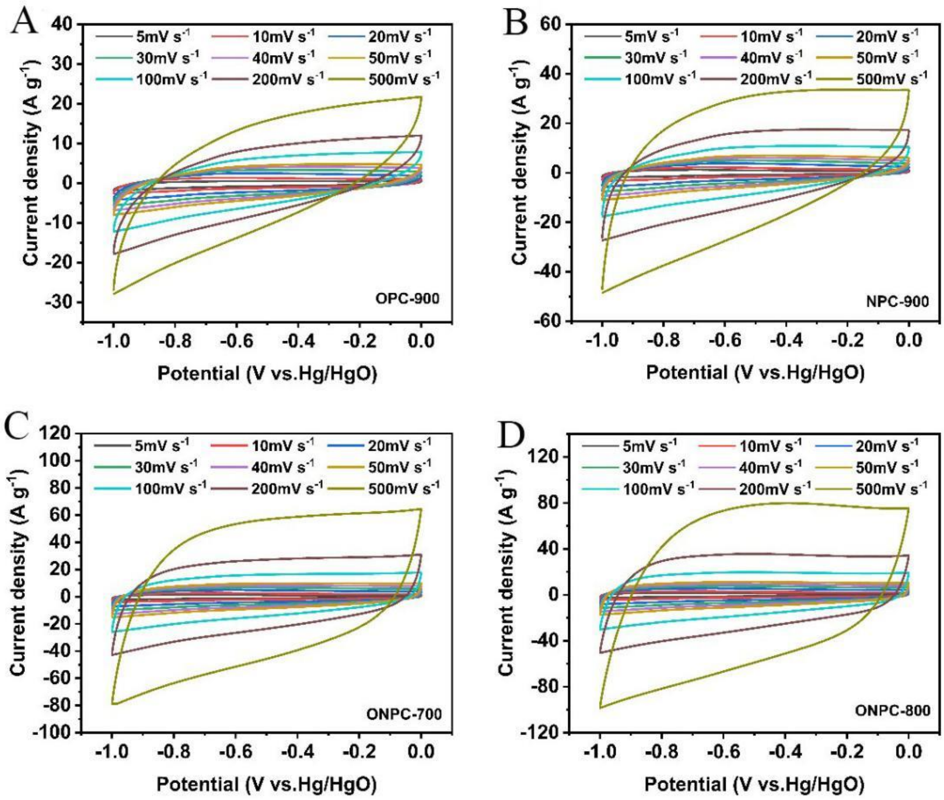

Figure 10. CV curves at various scans (5~500 mV s^{-1}) of (A) OPC-900; (B) NPC-900; (C) ONPC-700; and (D) ONPC-800, respectively.

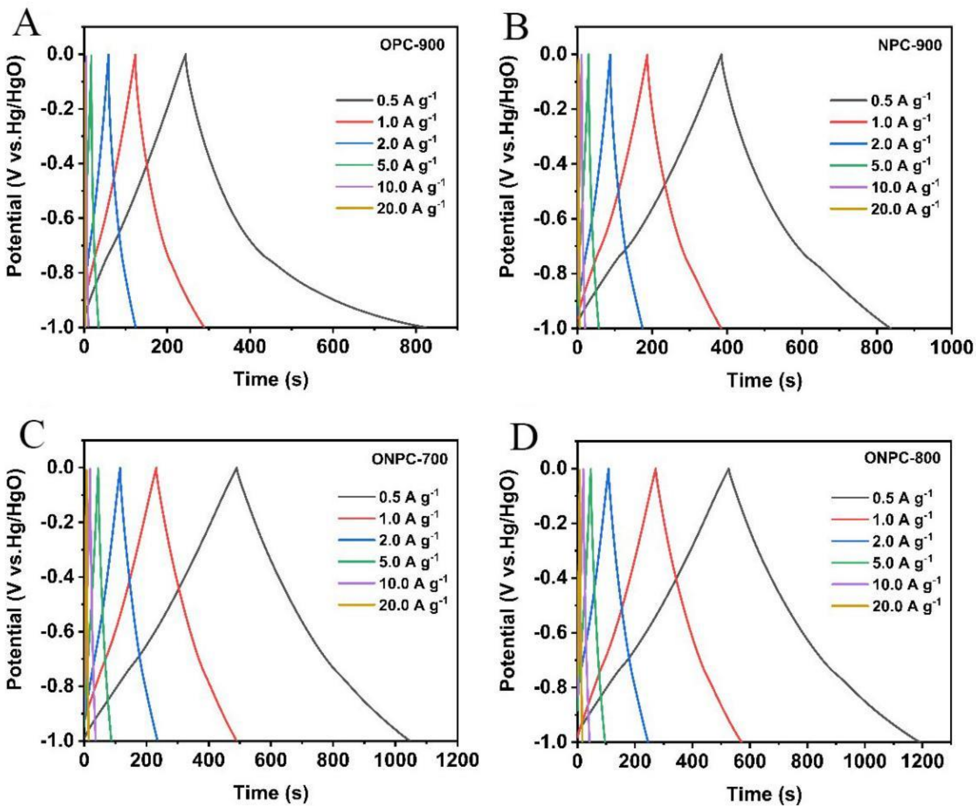

Figure 11. GCD curves of (A) OPC-900; (B) NPC-900; (C) ONPC-700; and (D) ONPC-800, respectively.

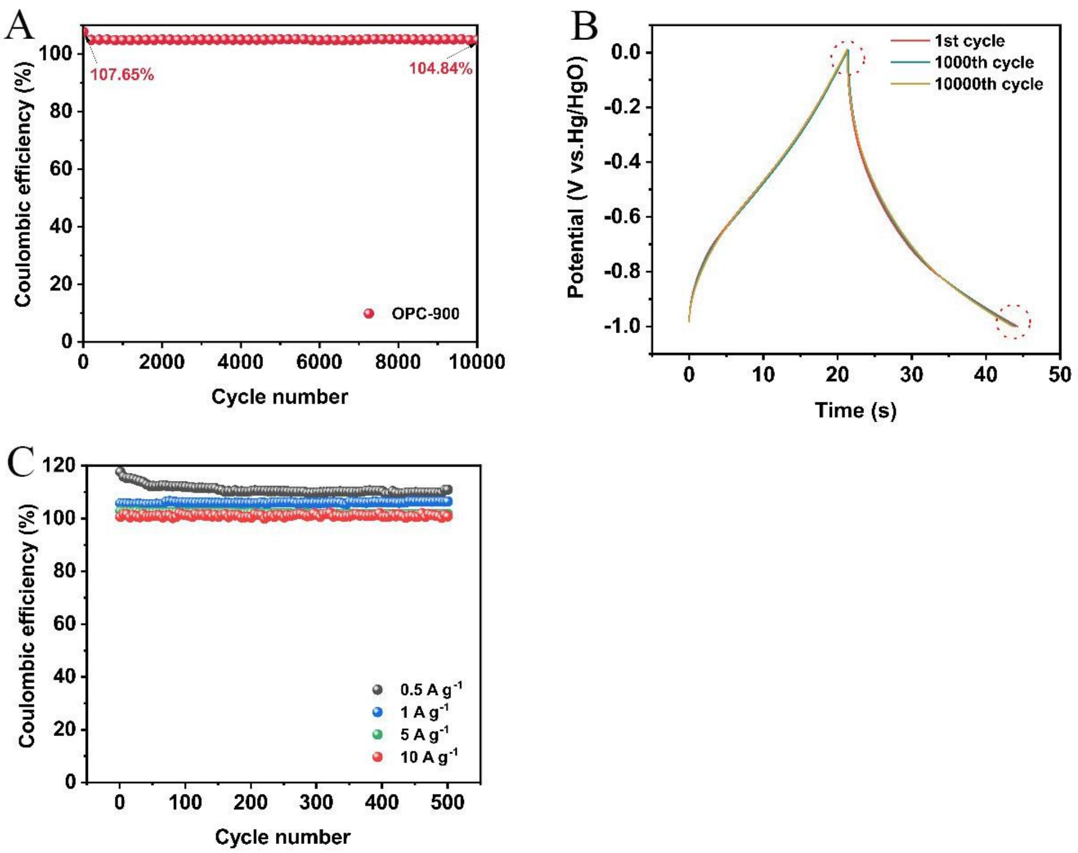

Figure 12. (A) Coulombic efficiency of OPC-900 after 10,000 cycles at 5 A g^{-1} in 6.0 mol L^{-1} KOH (three-electrode system); (B) GCD plots of OPC-900 at 1st, 1000th, and 10,000th cycle 5 A g^{-1} current density; (C) Coulombic efficiency of OPC-900 after 500 cycles at different current densities (0.5 A g^{-1}, 1 A g^{-1}, 5 A g^{-1}, and 10A g^{-1}) in 6.0 mol L^{-1} KOH (three-electrode system).

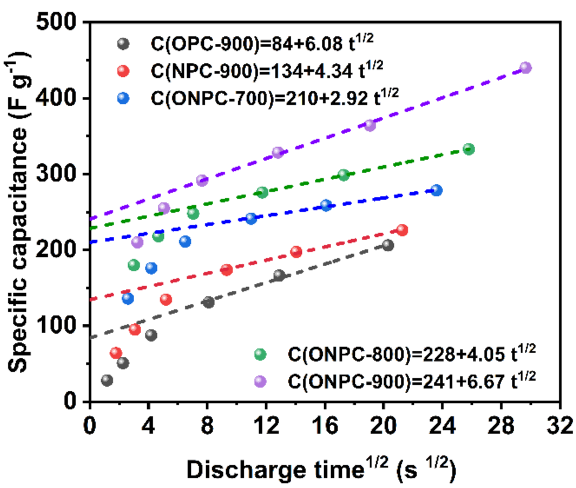

Figure 13. Capacity (C_t) of the ONPC electrode versus the square root of the discharge time.

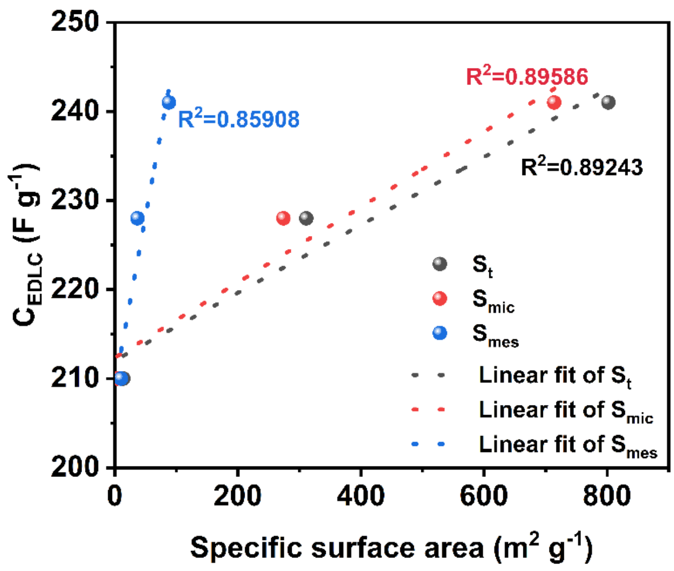

Figure 14. The relationship between surface areas (S_t, S_{mic} and S_{mes}) and C_{EDLC} of ONPC electrodes.

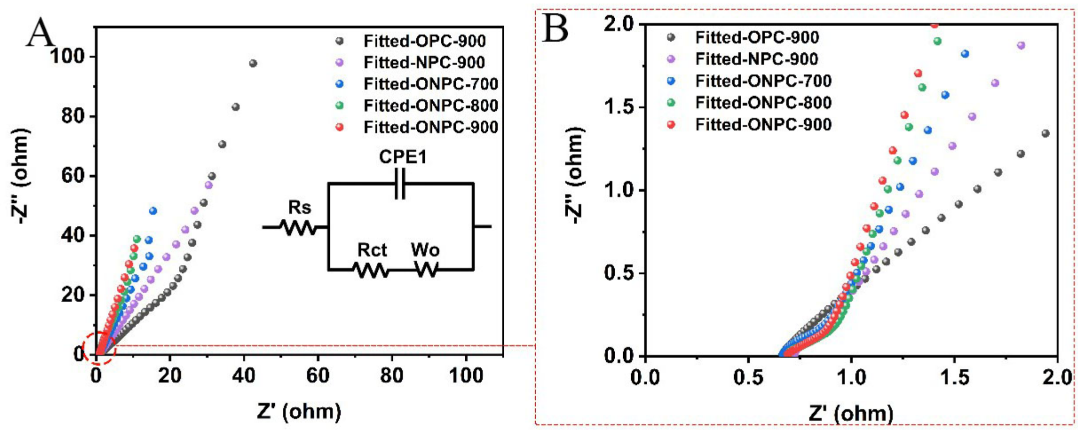

Figure 15. (A) The fitted impedance curves of all ONPC materials; inset is the equivalent circuit diagram of impedance; (B) The zoomed high-frequency region of the fitted Nyquist plots of all ONPC materials.

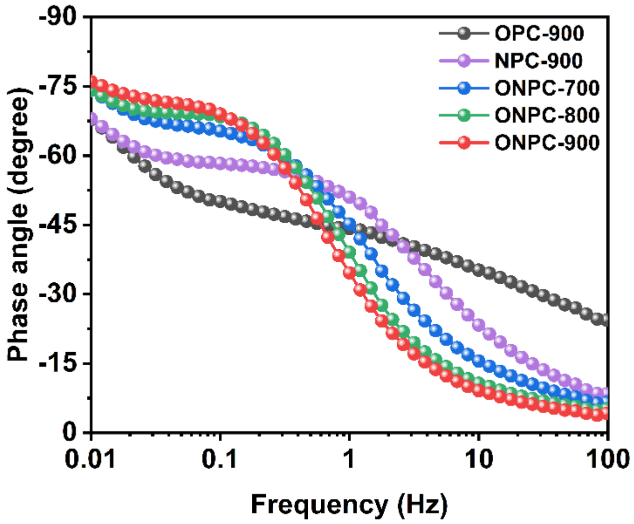

Figure 16. The Bode plots of all ONPC materials.

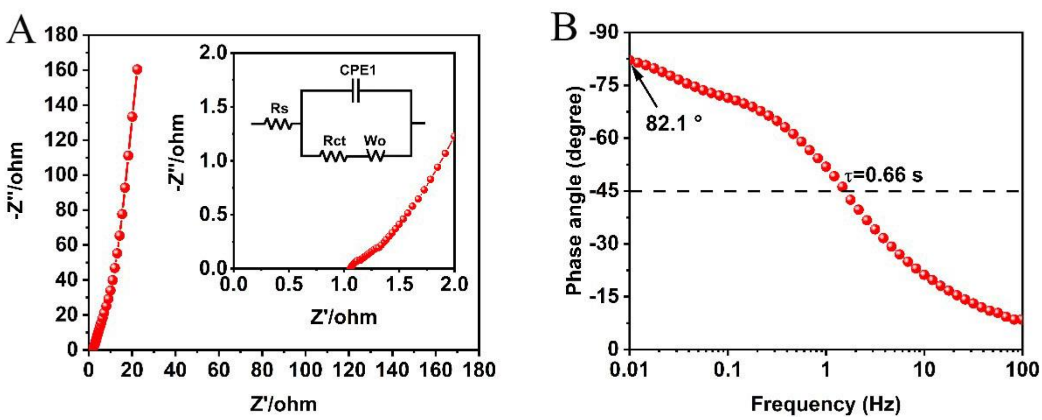

Figure 17. (A) Nyquist plot; (B) Bode phase diagrams of ONPC-900//ONPC-900 symmetrical capacitors.

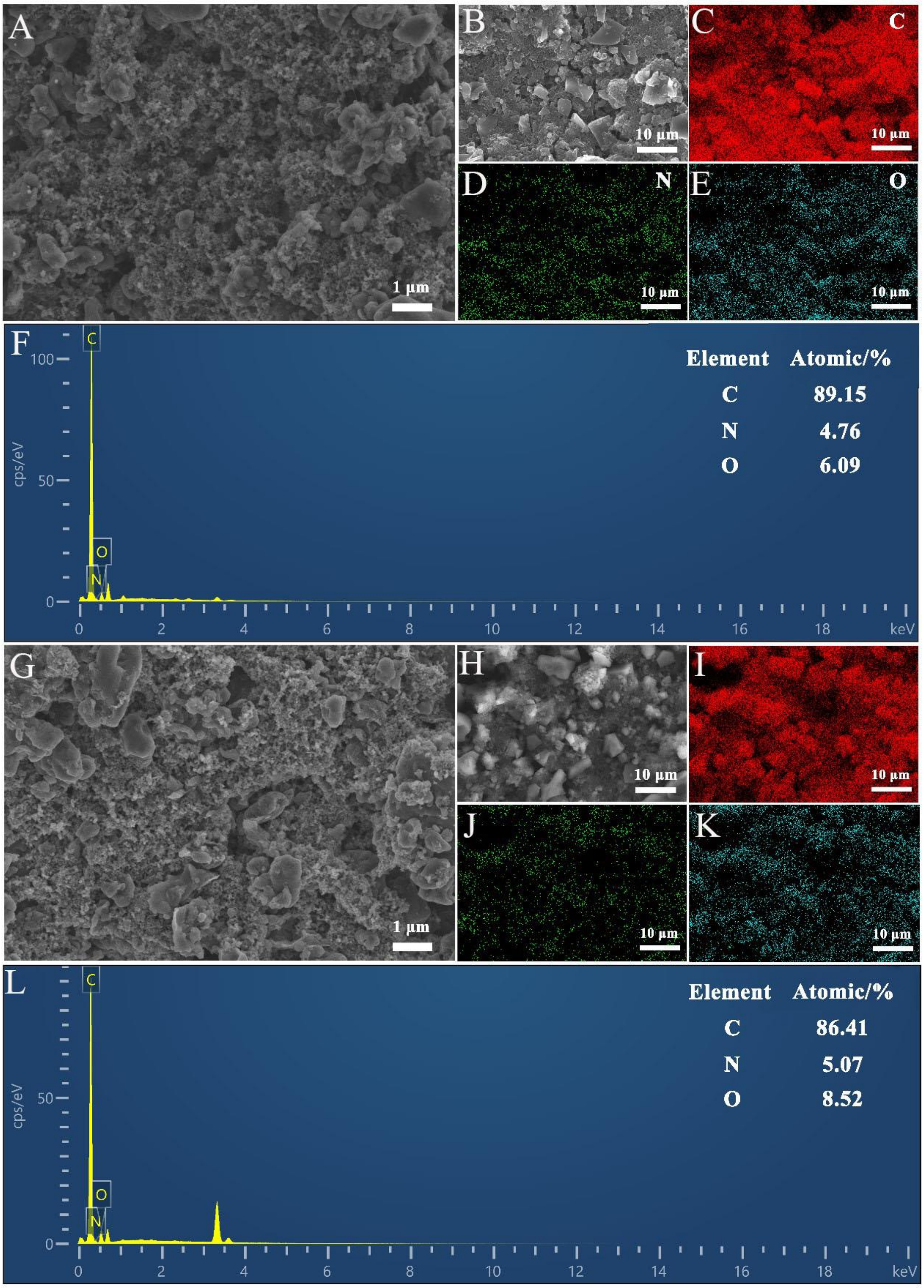

Figure 18. FESEM (A, G), EDS (F, L), and Mapping (B-E, H-K) of the ONPC-900 electrode before (A-F) and after(G-L) long cycle stability analysis.

Table 1. Proximate analysis and ultimate analysis of the raw lignite and pre-treated lignite

Sample	Proximate analysis (wt.%)				Ultimate analysis (t.%/daf)				
	M_{ad}	A_d	V_{ad}	FC_d	C_d	H_d	O_d	N_d	$S_{t,d}$
Raw lignite	8.42	10.18	34.28	52.39	64.32	3.32	21.36	0.70	0.13
Pre-treated lignite	6.45	0.54	38.87	54.18	65.20	4.17	24.62	0.65	0.22

ad: Air dried basis; d: dry base; daf: dry and ash-free base; M: moisture; A: ash; V: volatile matter; FC: fixed carbon.

Table 2. Collected dataset from previous works

#	SC (F g^{-1})	PW (V)	CD (A g^{-1})	C %	N %	O %	N-6 %	N-5 %	N-Q %	OI %	OII %	OIII %	SSA (m^2 g^{-1})	V_t (cm^3 g^{-1})	S_{mic} (m^2 g^{-1})	V_{mic} (cm^3 g^{-1})	Ref.
1	340	0.9	0.1	74.63	2.51	13.28	70.4	20.6	9	27.6	34.8	37.6	645	0.31	628	0.29	[S1]
2	309	0.9	0.1	80.82	1.39	9.95	34.1	38.8	27.1	21.4	58.2	20.4	1106	0.55	946	0.44	
3	253	0.9	0.1	87.04	0.95	5.55	44.6	18.8	36.6	39	23.3	37.7	1586	0.78	1296	0.6	
4	331	0.9	0.2	74.63	2.51	13.28	70.4	20.6	9	27.6	34.8	37.6	645	0.31	628	0.29	
5	298	0.9	0.2	80.82	1.39	9.95	34.1	38.8	27.1	21.4	58.2	20.4	1106	0.55	946	0.44	
6	229	0.9	0.2	87.04	0.95	5.55	44.6	18.8	36.6	39	23.3	37.7	1586	0.78	1296	0.6	
7	300	0.9	0.5	74.63	2.51	13.28	70.4	20.6	9	27.6	34.8	37.6	645	0.31	628	0.29	
8	278	0.9	0.5	80.82	1.39	9.95	34.1	38.8	27.1	21.4	58.2	20.4	1106	0.55	946	0.44	
9	208	0.9	0.5	87.04	0.95	5.55	44.6	18.8	36.6	39	23.3	37.7	1586	0.78	1296	0.6	
10	279	0.9	1	74.63	2.51	13.28	70.4	20.6	9	27.6	34.8	37.6	645	0.31	628	0.29	
11	269	0.9	1	80.82	1.39	9.95	34.1	38.8	27.1	21.4	58.2	20.4	1106	0.55	946	0.44	
12	200	0.9	1	87.04	0.95	5.55	44.6	18.8	36.6	39	23.3	37.7	1586	0.78	1296	0.6	
13	352	1	0.1	75.8	4.4	17.9	34.76	42.62	12.62	45.23	42.39	12.39	1949	0.88		0.68	[S2]
14	105	1	0.1	81	2.8	15.3	33.57	45.71	13.21	47.73	42.09	10.18	408	0.1		0.09	
15	269	1	0.1	79.8	1.1	16.2	54.12	25.29	15.88	29.13	54.13	16.75	1347	0.61		0.56	

#	SC (F g^{-1})	PW (V)	CD (A g^{-1})	C %	N %	O %	N-6 %	N-5 %	N-Q %	OI %	OII %	OIII %	SSA (m^2 g^{-1})	V_t (cm^3 g^{-1})	S_{mic} (m^2 g^{-1})	V_{mic} (cm^3 g^{-1})	Ref.
16	351	0.8	0.1	79.33	3.82	16.55	28.8	37.17	12.3	20.85	57.95	21.21	1610	0.86	1480	0.63	[S3]
17	342	0.8	0.1	81.2	2.46	15.99	30.89	26.83	15.85	5.44	62.91	31.58	2515	1.37	1553	0.84	
18	256	0.8	0.1	82.97	1.62	17.13	20.99	29.01	16.05	10.74	66.84	22.42	2605	1.41	1460	0.78	
19	292	0.8	0.1	83.31	1.35	15.03	16.3	36.3	16.3	16.37	70	13.64	3381	2.23	1128	0.6	
20	257	0.8	0.1	83.77	0.9	15.32	14.44	32.22	20	17.69	68.02	14.3	3430	2.27	1059	0.57	
21	244	0.8	1	79.33	3.82	16.55	28.8	37.17	12.3	20.85	57.95	21.21	1610	0.86	1480	0.63	[S4]
22	272	0.8	1	81.2	2.46	15.99	30.89	26.83	15.85	5.44	62.91	31.58	2515	1.37	1553	0.84	
23	220	0.8	1	82.97	1.62	17.13	20.99	29.01	16.05	10.74	66.84	22.42	2605	1.41	1460	0.78	
24	241	0.8	1	83.31	1.35	15.03	16.3	36.3	16.3	16.37	70	13.64	3381	2.23	1128	0.6	
25	227	0.8	1	83.77	0.9	15.32	14.44	32.22	20	17.69	68.02	14.3	3430	2.27	1059	0.57	
26	547	0.8	0.1	84.77	2.96	12.28	36.82	27.7	20.95	29.89	32.41	37.7	2209	1.2	1574	0.79	
27	337	0.8	0.1	85.83	2.45	11.72	29.8	24.08	24.9	29.18	40.61	30.2	2306	1.26	1556	0.76	
28	347	0.8	0.1	88.07	1.42	10.52	24.65	26.06	23.24	30.04	42.4	27.47	3147	1.85	1320	0.68	
29	288	0.8	0.1	90.89	0.69	8.43	21.74	26.09	17.39	22	44.6	34.16	3337	2.06	1283	0.65	
30	225	0.8	0.1	90.96	0.65	8.39	20	27.69	23.08	15.02	18.12	14.78	2713	1.81	1072	0.52	
31	374	1	0.2	83.15	2.73	14.11	15.89	61.67	18.9	9.13	69.06	21.81	2649	2.38		0.49	[S5]
32	260	1	0.2	93.28	1.63	5.09	37.5	44.74	12.36	11.92	47.81	40.27	1719	1.16		0.44	

#	SC ($F g^{-1}$)	PW (V)	CD ($A g^{-1}$)	C %	N %	O %	N-6 %	N-5 %	N-Q %	OI %	OII %	OIII %	SSA ($m^2 g^{-1}$)	V_t ($cm^3 g^{-1}$)	S_{mic} ($m^2 g^{-1}$)	V_{mic} ($cm^3 g^{-1}$)	Ref.
33	412.5	1	0.5	82.41	1.8	15.79	33.7	28.7	22	23.3	62.9	13.8	1488.3	1.286	1197.8		[S6]
34	182	1	1	83.4	7.9	8.67	50.53	23.98	14.09	24.17	69.99	5.84	11.62	0.021			[S7]
35	209	1	1	86.6	4.72	7.85	49.57	22.21	20.8	25.35	69.3	5.34	858.17	0.587			
36	421	1	1	83.04	5.61	9.83	49.51	19.87	9.28	24.17	74.27	1.56	911.12	0.415			
37	344	1	1	81.69	4.66	13.65	57.04	17.23	12.48	56.47	37.59	5.94	639.67	0.328			
38	217.5	1	1	72.7	5.5	21.8	45	1.15	51.07	2.52	95.91	1.57	46.17	0.059	31.92	0.0161	[S8]
39	358.6	1	1	80.53	5.03	14.44	61.99	18.91	14.98	19.12	77.75	3.13	145.39	0.1255	108.52	0.0559	
40	420.9	1	1	89.55	2.13	8.32	17.22	6.53	47.54	16.93	74.5	8.57	1223.82	0.8335	1002.8	0.5052	
41	275.9	1	1	84.01	5.02	10.98	53.66	16.57	12.57	18.83	72.87	8.3	506.75	1.4883	506.75	0.2212	
42	341	1	1	75.55	8.72	15.73	34.53	31.18	34.29	29.49	42.78	27.73	2128		1809		[S9]
43	402	1	1	82.93	6.9	10.17	59.68	24.94	15.39	36.56	38.29	25.15	2379		1976		
44	311	1	1	82.74	6.51	10.75	55.74	26.37	17.89	28.48	48.44	23.08	1921		1552		
45	200	1	1	75.73	10.23	14.04	31.86	33.45	34.69	22.13	48.01	29.86	690		562		
46	280	1	1	84.39	5.1	10.51	32.55	21.95	45.5	30.07	41.42	28.51	1782		779		
47	261	1	1	84.97	2.39	12.64	59.71	26.18	14.11	38.97	38.13	22.9	1247		443		
48	32	1	0.5	92.87	0.52	6.61	0	0	0	55	45	0	68	0.16		0.02	[S10]
49	279	1	0.5	97.6	0.35	2.05	0	0	0	51	49	0	2017	1.12		0.8	

#	SC (F g^{-1})	PW (V)	CD (A g^{-1})	C %	N %	O %	N-6 %	N-5 %	N-Q %	OI %	OII %	OIII %	SSA (m^2 g^{-1})	V_t (cm^3 g^{-1})	S_{mic} (m^2 g^{-1})	V_{mic} (cm^3 g^{-1})	Ref.
50	43	1	0.5	82.61	12.96	4.43	26	26	44	56	44	0	28	0.05		0.01	
51	297	1	0.5	94.52	3.55	1.93	29	40	16	52	48	0	1044	0.93		0.39	
52	367	1	0.5	95.17	3.01	1.82	42	20	29	34	66	0	1674	0.87		0.6	
53	299	1	0.5	95.98	2.17	1.85	34	31	24	42	58	0	1546	0.82		0.63	
54	187	1	0.5	96.22	1.95	1.83	36	15	34	36	64	0	1237	0.67		0.38	
55	115	1	0.5	96.47	1.86	1.67	49	10	30	47	53	0	1184	0.55		0.35	
56	286	1	0.5	95.88	2.15	1.97	41	18	33	41	59	0	1596	0.99		0.66	
57	186	0.8	1	77.94	11.64	10.41	16.99	39.92	24.73	27.76	46.37	25.87	1620	0.98	1331	0.62	[S11]
58	358	0.8	1	78.68	10.95	10.37	15.84	32.59	26.92	38.69	38.04	23.27	2660	1.54	2422	1.19	
59	267	0.8	1	81.19	6.15	12.66	16.63	24.22	30.5	23.29	40.02	36.69	2218	1.36	1938	0.98	
60	241	0.8	1	86.23	4.99	8.78	14.98	24.41	38.58	31.23	41.49	27.28	1527	1.01	1285	0.7	
61	256	0.8	1	80.65	8.57	10.78	23.24	22.75	30.76	47.92	30.43	21.65	1673	1.07	1389	0.71	
62	295	0.8	1	83.22	7.22	9.56	32.21	24.23	28.62	29.17	47.09	23.74	2144	1.21	1859	0.82	
63	275	0.8	1	79.04	5.76	15.2	26.15	25.16	30.98	46.55	31.41	43.27	2308	1.29	2134	1.01	
64	224	0.8	1	84	6.83	9.17	21.68	24.51	32.97	48.03	31.09	20.88	2536	1.31	2264	1.01	
65	279	0.8	1	75.72	7.89	16.4	30.61	31.5	23.41	45.51	33.48	21.01	2365	1.38	2027	0.94	
66	268	0.8	1	83.67	5.87	10.45	16.97	15.76	35.65	35.9	39.07	25.02	2714	1.42	2432	1.09	

#	SC (F g^{-1})	PW (V)	CD (A g^{-1})	C %	N %	O %	N-6 %	N-5 %	N-Q %	OI %	OII %	OIII %	SSA (m^2 g^{-1})	V_t (cm^3 g^{-1})	S_{mic} (m^2 g^{-1})	V_{mic} (cm^3 g^{-1})	Ref.
67	208	0.8	1	71.23	12.06	16.71	17.42	28.45	34.75	52.52	29.74	17.74	433	0.27	325	0.14	
68	245	0.8	1	76.28	11.23	12.48	32.21	24.23	28.62	70.64	29.36	0	1562	0.86	1118	0.45	
69	258	0.8	1	84.37	5.65	9.98	19.95	24.99	30.05	35.07	39.93	25	3112	1.63	2788	1.27	

Note: SC, Specific capacitance; PW, Potential Window; CD, current density; C%, Carbon atomic content; N%, nitrogen atomic content; O%, oxygen atomic content; N-5, Pyrrole nitrogen; N-6, Pyridine nitrogen; N-Q, Graphitic nitrogen; OI, C=O; OII, C-OH/C-O-C; OIII, -COOH; SSA, total specific surface area; S_{mic}, micropore specific surface area; V_t, total pore volume; V_{mic}, micropore volume. Ref.: #1-12[S1]; #13-15[S2]; #16-20[S3]; #21-30[S4]; #31-32[S5]; #33[S6]; #34-37[S7]; #38-41[S8]; #42-47[S9]; #48-56[S10]; #57-69 [S11];

Table 3. Pore parameters of all ONPC precursors

Samples	D_{ave}[a] nm	S_t[b] $m^2\ g^{-1}$	S_{mic}[c] $m^2\ g^{-1}$	S_{mes}[d] $m^2\ g^{-1}$	V_t[e] $cm^3\ g^{-1}$	V_{mic}[f] $cm^3\ g^{-1}$	V_{mes}[g] $cm^3\ g^{-1}$	V_{mic}/V_t %
$g\text{-}C_3N_4$	25	8	7	1	0.05	0.003	0.047	6%
Pre-treated lignite	8.89	9	2	7	0.02	0.001	0.019	5%

Note: a) D_{ave}, average pore diameter, D_{ave}= 4 V_t/S_{SSA}; b) S_t, total BET specific surface area; c) S_{mic}, micropore BET specific surface area; d) S_{mes}, Mesopore BET specific surface area; e) V_t, total pore volume; f) V_{mic}, micropore volume; g) V_{mes}, mesopore volume.

Table 4. Pore parameters of ONPC materials

Samples	D_{ave}[a] nm	S_t[b] $m^2\ g^{-1}$	S_{mic}[c] $m^2\ g^{-1}$	S_{mes}[d] $m^2\ g^{-1}$	V_t[e] $cm^3\ g^{-1}$	V_{mic}[f] $cm^3\ g^{-1}$	V_{mes}[g] $cm^3\ g^{-1}$	V_{mic}/V_t %
OPC-900	1.85	389	361	28	0.18	0.17	0.01	94%
NPC-900	1.94	309	275	34	0.15	0.13	0.02	87%
ONPC-700	2.86	14	4	10	0.01	0.002	0.008	20%
ONPC-800	1.80	311	274	37	0.14	0.13	0.01	93%
ONPC-900	1.84	802	714	88	0.37	0.34	0.03	92%

Note: a) D_{ave}, average pore diameter, D_{ave}= 4 V_t/S_{SSA}; b) S_t, total BET specific surface area; c) S_{mic}, micropore BET specific surface area; d) S_{mes}, Mesopore BET specific surface area; e) V_t, total pore volume; f) V_{mic}, micropore volume; g) V_{mes}, mesopore volume.

Table 5. Relative atomic contents of active species by fitting N1s and O1s XPS spectra for all obtained ONPC materials.

Samples	N 1s (at%)			O 1s (at%)			Active species (at%)
	N-6	N-5	N-Q	C=O	C-OH	-COOH	
OPC-900	0	0	0	4.21	4.16	8.17	12.33
NPC-900	1.85	1.31	1.11	2.07	2.08	3.32	6.71
ONPC-700	13.95	4.55	2.50	2.44	2.53	2.92	10.0
ONPC-800	5.40	2.12	0.91	5.73	3.04	3.62	8.78
ONPC-900	1.67	1.61	2.42	2.39	3.64	4.88	10.13

Table 6. Capacitances of ONPC electrodes

Samples	C_t (F g^{-1})	C_E (F g^{-1})	C_P (F g^{-1})	C_E/C_t (%)	C_P/C_t (%)
OPC-900	206	84	122	40.8	59.2
NPC-900	226	134	92	59.3	40.7
ONPC-700	278	210	68	75.5	24.5
ONPC-800	333	228	105	68.5	31.5
ONPC-900	440	241	199	54.8	45.2

C_t: the total electrochemical capacitance of ONPC electrodes at 0.5 A g^{-1} measured in a three-electrode system using 6 M KOH electrolyte; C_E: electric double-layer capacitance; C_P: pseudocapacitance.

Table 7. The calculated parameters of the equivalent circuit for the obtained materials

Sample	Rs (Ω)	Rct (Ω)	Wo-R	Wo-T	Wo-P
OPC-900	0.65	3.11	135.9	10.65	0.52
NPC-900	0.72	0.10	261.4	130.9	0.68
ONPC-700	0.66	0.32	255.3	99.12	0.76
ONPC-800	0.70	0.24	232.7	103.4	0.81
ONPC-900	0.68	0.03	0.54	0.10	0.42

Table 8. Comparisons of the power density and energy density for supercapacitors in this work and reported porous carbon materials from literature

Sample	Power density W kg^{-1}	Energy density Wh kg^{-1}	Cycling stability, Number of cycles, current density	Ref.
C-0.05N-700	25.2	8.1	100% (20,000, 10A g^{-1})	[S12]
MKHC-0.50	250	8.9	99% (10,000, 5A g^{-1})	[S13]
NCF-KOH	249.6	10.34	96% (10,000, 5A g^{-1})	[S14]
HPCNC-800-a	500	9.7	85% (5,000, 5A g^{-1})	[S15]
h-CPC	250	8.3	88% (10,000, 5A g^{-1})	[S16]
NPCA-MSC	251	6.8	91% (10,000, 1A g^{-1})	[S17]
NOCN900	250	6	92% (10,000, 5A g^{-1})	[S18]
PPC-5	125	10.35	95.3% (10,000, 1A g^{-1})	[S19]
PC/NC-L	125	8.03	95.3% (10,000, 5A g^{-1})	[S20]
N-C-HPCS	250	10.1	107.7% (10,000, 5A g^{-1})	[S21]
NOCN-850-3	175	12.3	97.6% (10,000, 10A g^{-1})	[S22]
TCF-UDSL	250	8.77	93% (10,000, 2A g^{-1})	[S23]
a-NSPC	50	14.76	97.44% (10,000, 1A g^{-1})	[S24]

Sample	**Power density W kg^{-1}**	**Energy density Wh kg^{-1}**	**Cycling stability, Number of cycles, current density**	**Ref.**
POCA800	125	8.07	94.6% (20,000, 10A g^{-1})	[S25]
MACN	250	10	93.7% (10,000, 10A g^{-1})	[S26]
CHPC900	125	9.9	96.2% (10,000, 1A g^{-1})	[S27]
NOPC-2	25000	14.5	94.3% (20,000, 10A g^{-1})	[S28]
RFN-KNa	703.4	17.42	91.6% (4,000, 5A g^{-1})	[S29]
MSAC-4	162.5	14.04	80% (10,000, 5A g^{-1})	[S30]
N–HNC	500	15.99	95.74% (10,000, 10A g^{-1})	[S31]
N–HNC3-1	220	7	--	[S32]
PCNs/GCNs-5	464.06	24.75	98% (5,000, 1A g^{-1})	[S33]
HPC	100	10.93	92.3% (10,000, 1A g^{-1})	[S34]
NOCS-1/10	250	4.33	97% (10,000, 5A g^{-1})	[S35]
ONPC-900	250	10.8	93.8% (30,000, 5 A g^{-1})	This work

REFERENCES

S1. Wang K, Zhao N, Lei SW, et al. Promising biomass-based activated carbons derived from willow catkins for high performance supercapacitors. *Electrochim Acta* 2015;166:1-11. https://doi.org/10.1016/j.electacta.2015.03.048

S2. Guo NN, Li M, Wang Y, Sun XK, Wang F, Yang R. N-Doped hierarchical porous carbon prepared by simultaneous-activation of KOH and NH3 for high performance supercapacitors. *RSC Adv* 2016;6:101372-101379. https://doi.org/10.1039/C6RA22426A

S3. Zhao ZJ, Wang Y, Li M, Yang R. High performance N-doped porous activated carbon based on chicken feather for supercapacitors and CO2 capture. *RSC Adv* 2015;5:34803-34811. https://doi.org/10.1039/C5RA01569C

S4. Wang Y, Yang R, Wei Y, Zhao ZJ, Li M. Preparation of novel pigskin-derived carbon sheets and their low-temperature activation-induced high capacitive performance. *RSC Adv* 2014;4:45318-45324. https://doi.org/10.1039/C4RA08055F

S5. Zhang XK, Ma XQ, Yu ZS, Yi YJ, Lu CX, Lu XL. Microwave-assisted two-step pyrolysis of water hyacinth for the preparation of N-self-doped porous carbon. *J Anal Appl Pyrolysis* 2023;173:106061. https://doi.org/10.1016/j.jaap.2023.106061

S6. Wang YH, Liu RN, Tian YD, et al. Heteroatoms-doped hierarchical porous carbon derived from chitin for flexible all-solid-state symmetric supercapacitors. *Chem Eng J* 2020;384:123263. https://doi.org/10.1016/j.cej.2019.123263

S7. Liu PY, Xing ZH, Wang X, et al. Nanoarchitectonics of nitrogen-doped porous carbon derived from leather wastes for solid-state supercapacitor. *J Mater Sci Mater Electron* 2022;33:4887-4901. https://doi.org/10.1007/s10854-021-07678-5

S8. Zhang HM, Xue JY, Wang S, Song Y, Zhao JP, Li Y. Fabrication of high density and nitrogen-doped porous carbon for high volumetric performance supercapacitors. *J Energy Storage* 2022;47:103657. https://doi.org/10.1016/j.est.2021.103657

S9. Song ZY, Li LC, Zhu DZ, et al. Synergistic design of a N, O co-doped honeycomb carbon electrode and an ionogel electrolyte enabling all-solid-state supercapacitors with an ultrahigh energy density. *J Mater Chem A* 2019;7:816-826. https://doi.org/10.1039/C8TA10406A

S10. Guo DD, Xin RR, Wang YF, et al. N-doped carbons with hierarchically micro- and mesoporous structure derived from sawdust for high performance supercapacitors. *Microporous Mesoporous Mater* 2019;279:323-333. https://doi.org/10.1016/j.micromeso.2019.01.003

S11. Song ZY, Zhu DZ, Li LC, et al. Ultrahigh energy density of a N, O codoped carbon nanosphere based all-solid-state symmetric supercapacitor. *J Mater Chem A* 2019;7:1177-1186. https://doi.org/10.1039/C8TA10158B
S12. Chen P, Tang YK, Gao Y, Zhang Y, Liu L. Design and structure optimization of coal-based hierarchical porous carbon by molten salt method for high-performance supercapacitors. *J Power Sources* 2023;580. https://doi.org/10.1016/j.jpowsour.2023.233334
S13. Guo NN, Liu AJ, Luo WX, et al. Hybrid nanoarchitectonics of coal-derived carbon with oxidation-induced morphology-selectivity for high-performance supercapacitor. *J Colloid Interface Sci* 2023;639:171-179. https://doi.org/10.1016/j.jcis.2023.02.067
S14. Yang NN, Ji L, Fu HC, et al. Hierarchical porous carbon derived from coal-based carbon foam for high-performance supercapacitors. *Chinese Chem Lett* 2022;33:3961-3967. https://doi.org/10.1016/j.cclet.2022.03.037
S15. Shao JQ, Song MY, Wu G, et al. 3D carbon nanocage networks with multiscale pores for high-rate supercapacitors by flower-like template and in-situ coating. *Energy Storage Mater* 2018;13:57-65. https://doi.org/10.1016/j.ensm.2017.12.023
S16. Cai LM, Zhang YZ, Ma R, et al. Nitrogen-doped hierarchical porous carbon derived from coal for high-performance supercapacitor. *Molecules* 2023;28:3660. https://doi.org/10.3390/molecules28093660
S17. Gao YF, Zheng SH, Fu HL, et al. Three-dimensional nitrogen doped hierarchically porous carbon aerogels with ultrahigh specific surface area for high-performance supercapacitors and flexible micro-supercapacitors. *Carbon* 2020;168:701-709. https://doi.org/10.1016/j.carbon.2020.06.063
S18. Ran FT, Yang XB, Xu XQ, Li SW, Liu YY, Shao L. Green activation of sustainable resources to synthesize nitrogen-doped oxygen-riched porous carbon nanosheets towards high-performance supercapacitor. *Chem Eng J* 2021;412. https://doi.org/10.1016/j.cej.2021.128673
S19. Dong D, Zhang YS, Xiao Y, Wang T, Wang JW, Gao W. Oxygen-enriched coal-based porous carbon under plasma-assisted $MgCO_3$ activation as supercapacitor electrodes. *Fuel* 2022;309. https://doi.org/10.1016/j.fuel.2021.122168
S20. Zhang ZQ, Li YD, Yang XM, et al. In-situ confined construction of N-doped compact bamboo charcoal composites for supercapacitors. *J Energy Storage* 2023;62. https://doi.org/10.1016/j.est.2023.106954

S21. Park S, Seo B, Shin D, Kim K, Choi W. Sodium-chloride-assisted synthesis of nitrogen-doped porous carbon shells via one-step combustion waves for supercapacitor electrodes. *Chem Eng J* 2022;433:134486. https://doi.org/10.1016/j.cej.2021.134486
S22. Liu ZS, Qin AM, Zhang KY, Lian P, Yin XD, Tan H. Design and structure of nitrogen and oxygen co-doped carbon spheres with wrinkled nanocages as active material for supercapacitor application. *Nano Energy* 2021;90:106540. https://doi.org/10.1016/j.nanoen.2021.106540
S23. Wang GP, Hu GD, Lan J, Miao FJ, Zhang P, Shao GS. Rational design of one-dimensional skin-core multilayer structure for electrospun carbon nanofibers with bicontinuous electron/ion transport toward high-performance supercapacitors. *J Colloid Interface Sci* 2024;653:148-158. https://doi.org/10.1016/j.jcis.2023.09.064
S24. Li G, Chen SS, Wang YG, Wang G, Wu YH, Xu Y. N, S co-doped porous graphene-like carbon synthesized by a facile coal tar pitch-blowing strategy for high-performance supercapacitors. *Chem Phys Lett* 2023;827:140712. https://doi.org/10.1016/j.cplett.2023.140712
S25. Yang XX, Sun GX, Wang F, et al. Rational design of dense microporous carbon derived from coal tar pitch towards high mass loading supercapacitors. *J Colloid Interface Sci* 2023;646:228-237. https://doi.org/10.1016/j.jcis.2023.04.179
S26. Dong D, Zhang YS, Xiao Y, et al. High performance aqueous supercapacitor based on nitrogen-doped coal-based activated carbon electrode materials. *J Colloid Interface Sci* 2020;580:77-87. https://doi.org/10.1016/j.jcis.2020.07.018
S27. Dong D, Xiao Y, Xing JY. Facile wet mechanochemistry coupled K_2FeO_4 activation to prepare functional coal-derived hierarchical porous carbon for supercapacitors. *J Cleaner Prod* 2023;428:139474. https://doi.org/10.1016/j.jclepro.2023.139474
S28. Hou LQ, Yang W, Li Y, et al. Dual-template endowing N, O co-doped hierarchically porous carbon from potassium citrate with high capacitance and rate capability for supercapacitors. *Chem Eng J* 2021;417:129289. https://doi.org/10.1016/j.cej.2021.129289
S29. Liu D, Liu YL, Xu GY, Ding YG, Fan BM, Li HY. Precisely tuning porosity and outstanding supercapacitor performance of phenolic resin-based carbons via citrate activation. *J Energy Storage* 2023;67:107610. https://doi.org/10.1016/j.est.2023.107610

S30. Lu SS, Yang WS, Zhou M, et al. Nitrogen-and oxygen-doped carbon with abundant micropores derived from biomass waste for all-solid-state flexible supercapacitors. *J Colloid Interface Sci* 2022;610:1088-1099. https://doi.org/10.1016/j.jcis.2021.11.164
S31. Shang Z, An XY, Zhang H, et al. Houttuynia-derived nitrogen-doped hierarchically porous carbon for high-performance supercapacitor. *Carbon* 2020;161:62-70. https://doi.org/10.1016/j.carbon.2020.01.020
S32. Deng XY, Zhu S, Li JJ, et al. Bio-inspired three-dimensional carbon network with enhanced mass-transfer ability for supercapacitors. *Carbon* 2019;143:728-735. https://doi.org/10.1016/j.carbon.2018.11.055
S33. Zhang GL, Zhang Y, Wang JL, et al. Nitrogen-functionalization of carbon materials for supercapacitor: combining with nanostructure directly is superior to doping amorphous element. *J Colloid Interface Sci* 2024;660:478-489. https://doi.org/10.1016/j.jcis.2024.01.112
S34. Qian XY, Miao L, Jiang JX, et al. Hydrangea -like N/O codoped porous carbons for high-energy supercapacitors. *Chem Eng J* 2020;388:124208. https://doi.org/10.1016/j.cej.2020.124208
S35. Zhang R, Jing XX, Chu YT, et al. Nitrogen/oxygen co-doped monolithic carbon electrodes derived from melamine foam for high-performance supercapacitors. *J Mater Chem A* 2018;6:17730-17739. https://doi.org/10.1039/C8TA06471G